International Journal of Computer Assisted Radiology and Surgery (2020) 15:403–413
https://doi.org/10.1007/s11548-020-02116-z

ORIGINAL ARTICLE

Modified radial-search algorithm for segmentation of tibiofemoral cartilage in MR images of patients with subchondral lesion

Rafeek Thaha[1] · Sandeep P. Jogi[1,2] · Sriram Rajan[3] · Vidur Mahajan[3] · Vasantha K. Venugopal[3] · Amit Mehndiratta[1,4] · Anup Singh[1,4]

Received: 8 August 2019 / Accepted: 6 January 2020 / Published online: 11 January 2020

Abstract

Purpose The quantitative analysis of weight-bearing articular cartilage superficial to subchondral abnormality is important in osteoarthritis (OA) progression studies. The current study aimed to address the challenges of a semi-automatic segmentation of tibiofemoral cartilage in MR images of OA patient with and without subchondral bone abnormalities (SBA).

Methods In this study, knee MRI data [fat-suppressed proton density-weighted, multi-echo T2-weighted (CartiGram) images] of 29 OA patients, acquired at 3.0T MR scanner, were retrospectively collected. Out of 29 data, 9 had SBA in femur bone. Initially, a semi-automatic femur cartilage segmentation based on radial intensity search approach by Akhtar et al. was implemented in-house. This algorithm was considered as the radial-search method for further comparison. In this current study, the reported radial-search (RS)-based semi-automatic cartilage segmentation method was modified using thresholding, connected component labelling, convex-hull operation and spline-based curve fitting for the improved segmentation of tibiofemoral cartilage. Cartilage was manually segmented by two experienced radiologists, and inter-reader variability was estimated using coefficient of variation (CV). The segmentation results were validated using dice coefficient (DC), Jaccard coefficient (JC) and sensitivity index measurements.

Results DC values for segmented femur cartilage in patients with SBA were $64.6 \pm 7.8\%$ and $81.4 \pm 2.8\%$ using reported RS method and modified radial-search method, respectively. DC values for segmented femur cartilage in patients without SBA were $82.5 \pm 4.5\%$ and $84.8 \pm 2.0\%$ using RS method and modified radial method, respectively. Similarly, DC values for tibial cartilage in all OA patients were $80.4 \pm 1.6\%$ and $81.9 \pm 2.4\%$ using RS method and modified radial method, respectively. Similar segmentation results were also obtained from the T2-weighted images. Inter-reader variability result based on CV in femur cartilage was $3.40 \pm 2.12\%$ (without SBA) and $4.18 \pm 3.18\%$ (with SBA).

Conclusion In the current study, a semi-automated segmentation of tibiofemoral cartilage was presented. Modified radial-search approach can successfully segment tibiofemoral cartilage, and the results were tested and validated on knee MRI data of OA patients with and without SBA.

Keywords Articular cartilage · Osteoarthritis · MRI · Segmentation · Subchondral bone abnormality

Introduction

Osteoarthritis (OA) is a degenerative disorder of elder population and primarily associated with degradation of articular cartilage [1]. Magnetic resonance (MR) imaging is playing an important role in *non-invasive* imaging of soft tissues in the knee joint, particularly cartilage, ligaments and meniscus [2]. MR images help in understanding the morphological and biochemical properties of these tissues as well as in evaluating any changes in these properties associated with diseases like OA for which reliable segmentation of the cartilage is important. Subsegmentation of cartilage into

✉ Anup Singh
anups.minhas@gmail.com

1 Centre for Biomedical Engineering, Indian Institute of Technology Delhi, Room No: 299, Block – II, New Delhi, India

2 Department of Biomedical Engineering, ASET, Amity University Haryana, Gurgaon, India

3 Mahajan Imaging Centre, New Delhi, India

4 Department of Biomedical Engineering, All India Institute of Medical Sciences, New Delhi, India

weight bearing *vs* non-weight bearing as well as into deep *vs* superficial zones can play an important role in diagnosis. Subsequently, generation of a 2D flattened map (WearMap) from the entire segmented cartilage can be used as a visualization tool for understanding and evaluating the progression of the disease.

The main challenges of segmentation of cartilage are the poor contrast with respect to adjacent tissues, laminar structure, curved shape and small thickness [3]. Generally, in clinical practice, manual segmentation is performed for evaluating cartilage properties, which is subjective and a tedious task. Thus, the development of semi-automatic or automatic methods is useful for fast and reproducible segmentation. Reported automatic cartilage segmentation methods were broadly classified into model/atlas-based, edge/threshold-based and machine learning-based approaches. Akhtar et al. [4] reported a semi-automatic radial-search-based femur cartilage segmentation framework for high-resolution images of healthy subjects as well as OA patient data without any subchondral abnormality. In this study, the reported sensitivity of segmentation for healthy subjects and patient data with OA was $93.9 \pm 3.1\%$ and $71.1 \pm 2.9\%$, respectively. Recently, Liukkonen et al. [5] presented a radial intensity profile-based semi-automatic segmentation method for biomechanical modelling of the knee joint. However, this method was validated on MRI data of only six healthy subjects.

Reported radial-search-based semi-automatic segmentation method shows better performance with excellent soft tissue contrast producing MR sequences; however, this approach might fail in case of patient data having any subchondral bone abnormalities (SBA) [4–6]. Common SBA such as bone marrow oedema (BME)-like lesion are considered as one of the advanced characteristics of OA. BME-like lesions comprise of some of the non-characteristic histologic abnormalities that include bone marrow necrosis, bone marrow fibrosis, subchondral cysts and trabeculae abnormalities [7]. In SBA patients, there is a chance of overlapping the part of subchondral lesion area with the chondral area superficial to the abnormality. Studies show that severe OA condition is closely related to higher prevalence and greater volume of associated BME; therefore, the quantitative analysis of chondral area superficial to the SBA is important in OA progression studies [7].

Reported radial-search method has been tested on high-resolution fat-suppressed proton density fast spin echo (FS-PD-FSE) and fat-suppressed spoiled gradient recalled (FS-SPGR) sequences. These sequences are suitable for evaluating structural changes in the cartilage tissues. The presence of BME lesion, osteophytes formation and detection of joint bodies were often best seen on fast spin echo (FSE) MR sequences [2]. T2-weighted FSE images are primarily used for identifying the cartilage degenerative changes, whereas on these images sometimes it is difficult to find the presence of fibrillation and surface defects of the cartilage. However, T2 map developed from T2-weighted images is more sensitive to the biochemical information of the cartilage [8, 9].

In the current study, a semi-automatic framework based on modified radial-search algorithm is proposed for cartilage segmentation in OA patients with and without SBA. The proposed segmentation approach was tested on FS-PD-FSE-weighted images and multi-echo T2-weighted FSE images without fat saturation.

Methods

Subjects

In this study, MRI data set of 29 OA patients was collected retrospectively. These MRI data sets were collected as a part of routine clinical examination of OA patients. Of all patients, 9 patients had femoral abnormality. The subjects description and SBA class are given in Table 1.

Table 1 OA patient description and class of subchondral abnormality

SI no.	Age (years)	Sex	Weight (Kg)	SBA type	Affected bone
1	47	Male	90	Subchondral cystic change	Femur
2	59	Male	78	BME-like lesion and diffuse marrow change	Femur
3	29	Male	72	Small area of avascular necrosis	Femur
4	35	Female	48	BME-like lesion and cystic change	Femur
5	24	Male	75	Subchondral cystic change	Femur
6	41	Female	80	Subchondral cystic change and oedema	Femur
7	32	Male	79	Marginal osteophytes, subchondral cystic change	Femur
8	33	Male	76	Subchondral oedema and subchondral sclerosis	Femur
9	34	Male	70	Subtle subchondral oedema (BME)	Femur

Data acquisition

MRI data for knee joint were acquired using 3.0T MR scanner (General Electric healthcare, Chicago, Illinois) and eight-channel transmit/receive phase array knee coil. MRI protocol included acquisition of multiple slices of FS-PD-FSE-weighted and multi-echo T2-weighted (CartiGram) images in sagittal orientation for all patients and in coronal orientation for 18 patients data. MRI protocol for FS-PD-FSE-weighted images was: repetition time (TR) = 3000 ms, echo time (TE) = 27 ms, slice thickness = 4 mm, field of view (FOV) = 140×140 mm^2, number of slices = 14 to 16. MR protocol for T2-weighted FSE images was: TR = 1000 ms, TE = 6.4, 12.8, 19.2, 25.6, 32, 38.4, 44.8, 51.2 ms, slice thickness = 3 mm, FOV = 140×140 mm^2, number of slices = 10 to 12 containing cartilage.

Subjects were positioned supine inside the scanner, and the data acquisition was performed successively without any movement in the subject position. Rectangular-shaped foam pads were inserted into the knee coil to reduce any movement during scanning.

Data processing

The complete data processing was carried out by using in-house developed routines in MATLAB 2016b (The MathWorks Inc., Natick, MA, USA 2016). All the processing was performed on images acquired in sagittal orientation. Manual segmentation of cartilage for all the subjects was performed on FS-PD-FSE-weighted images by 2 experienced radiologists with 15 and 6 years of clinical experience for evaluating accuracy of cartilage segmentation. T2-weighted images were registered with FS-PD-FSE-weighted images.

Segmentation

First of all, reported radial-search-based cartilage segmentation method by Akhtar et al. [4] was implemented in-house. This algorithm was considered as the radial-search method for further comparison throughout this manuscript.

In the current study, a novel modified radial-search method has been proposed with the following steps:

(a) Initial thresholding process.
(b) Connected component labelling operation for the removal of small isolated SBA regions present in the subchondral area.
(c) Selection of seed points and inner boundary threshold value.
(d) Radial-search method for the detection of inner and outer boundary points.
(e) Two-step Otsu's thresholding operation to remove the other tissue part from the cartilage.
(f) Convex-hull and spline fitting operations to remove any leftover non cartilage tissues.
(g) Finally, tibiofemoral segmentation mask overlays on the FS-PD-FSE image.

In the current study, steps (b) and (f) are the major modifications to the radial-search method for segmentation of cartilage. The detailed description of the segmentation process is explained below:

(a) *Initial thresholding process*: In the modified radial-search method, two pre-processing steps were used successively on all the images before applying the radial line search inner–outer boundary recognition algorithm. The first operation is initial thresholding operation (Fig. 1b), and it was based on a threshold value (Thresh-1). The mean of the central slice image after removing the background noise was selected as Thresh-1.
(b) *Connected component labelling operation for the removal of small isolated SBA regions present in the subchondral area*: The connected component labelling operation (second pre-processing step) was used to remove all the small patches present in the image (Fig. 1h). It includes the heterogeneous contrast present in the condyle surfaces or closer to the bone–cartilage boundary, which might be present in OA patient data mainly due to SBA.
(c) *Selection of seed points and inner boundary threshold value*: From the acquired data, radial line search algorithm was initiated from the seed point. For the femoral cartilage segmentation, a single seed point (SP1) was obtained from the central slice of lateral compartment. For obtaining this seed point (SP1), two pixels were manually selected on the anterior and posterior superior osteochondral junctions of lateral compartment. The mid-point of line joining these two manually selected pixels was considered as the seed point (SP1). Similarly, for the tibial cartilage segmentation, a single seed point (SP2) was obtained from the central slice of lateral compartment. For obtaining the seed point (SP2), two pixels were manually selected on the anterior and posterior inferior osteochondral junctions. The mid-point of line joining these two manually selected pixels was considered as the seed point (SP2). In this algorithm, the initial threshold value (Thresh-1, as described in pre-processing stage) was selected as the inner cartilage boundary condition.
(d) *Radial-search method for the detection of inner and outer boundary points*: From the seed pixel $R\ (X_0, Y_0)$ selected by the user, the outward radial search starts for finding the inner threshold intensity value (Thresh-1) of cartilage boundary. The total angle of search varies

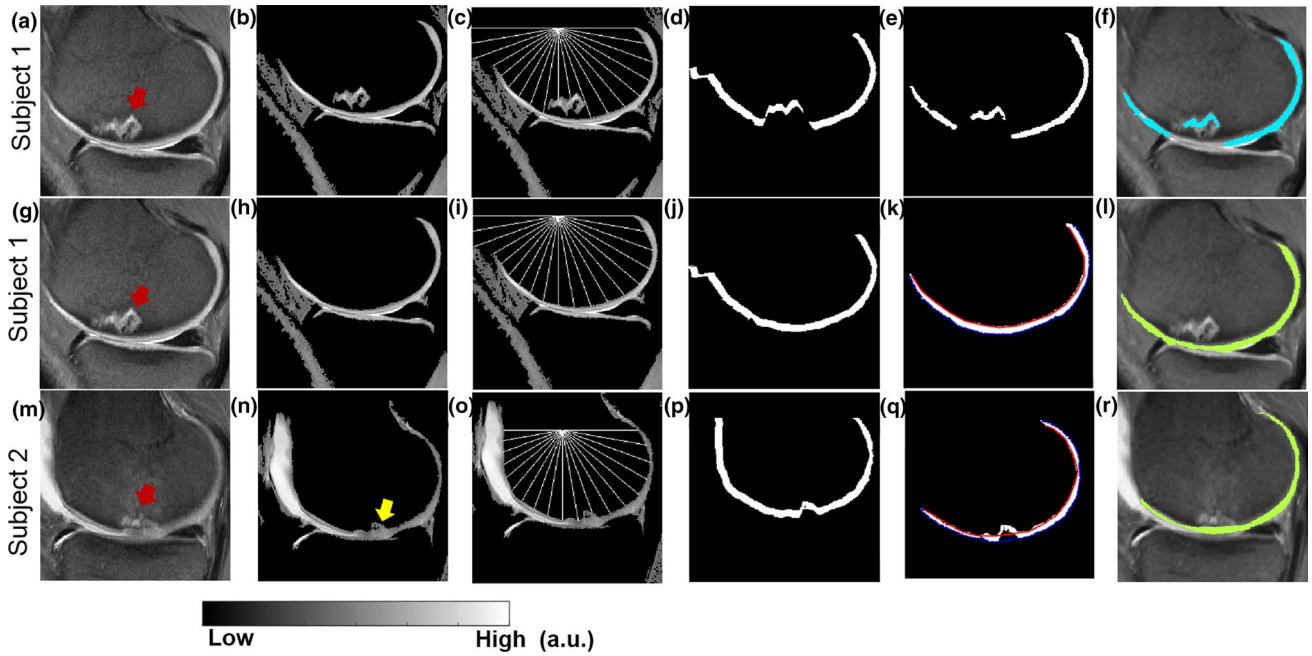

Fig. 1 Key steps of the cartilage segmentation workflow for 2 OA patients (subjects 1 and 2) having subchondral abnormality (SBA) using radial-search method (**a**–**f**), the proposed method (**g**–**l**) with subject 1 and the proposed method (**m**–**r**) with subject 2. Image **a** shows the FS-PD-FSE image of subject 1 having subchondral bone abnormality (indicated by red arrow), **b** shows the result of initial thresholding operation, **c** shows the representation of radial-search algorithm, **d** shows the generated mask (mask 1) after connecting the boundary points, **e** shows the result of two-step Otsu's thresholding, and **f** shows the femoral segmentation mask overlaid on FS-PD-FSE image. Key steps in the modified method are connected component labelling operation (**h**, **n**), convex-hull and spline interpolation-based curve fitting process (**k**, **q**). Yellow arrow in image (n) indicates the presence of merged subchondral lesion area to the superficial cartilage. The scale shows the intensity of FS-PD-FSE images and (a.u.) represents arbitrary unit

from 0° to 180° with an increment of $n°$ ($n=4$ was used in the current study), and the radial line search was performed using the following expression:

$$X_p(\theta) = X_0 + r_p \cos\theta \tag{1}$$

$$Y_p(\theta) = Y_0 + r_p \sin\theta \tag{2}$$

where X_p and Y_p are the pixel coordinate values of each radial-search line; $p=1, 2, 3\ldots P$, P is the end point of each radial line; $\theta=0, n, 2n, 3n\ldots, (N-1)n$; and $N=(180/n)$ is the number of radial searches in the image.

In each search, if the searching pixel intensity matches with the inner threshold value, the search stopped and the pixel coordinate R (X_{ip}, Y_{ip}) saved as inner boundary points (Fig. 1i). For obtaining the outer boundary point of cartilage R (X_{op}, Y_{op}), a fixed boundary length was initially used as ending condition. Fixed boundary length was assessed based on the resolution and average maximum possible thickness of femur–tibia cartilage in healthy volunteers [10]. In this study, it was taken as 4 mm each for femur and tibial cartilage. A mask (mask-1) was created by connecting points of inner and outer boundary (Fig. 1j). In addition to cartilage tissue, part of other tissues such as synovial fluid, meniscus, Hoffa's fat pad and joint capsule was also present inside mask-1, which were removed using thresholding operation described in the next step

(e) *Two-step Otsu's thresholding*: In this step, the generated mask was applied on corresponding FS-PD-FSE image. Two-step Otsu's thresholding operations were performed sequentially for the removal of intensities from other tissues. In the first stage, the tissues having high intensity values compared to cartilage such as synovial fluid area were removed by setting pixel value greater than Otsu's threshold level (level 1) equal to zero. From the obtained result, the remaining Hoffa's fat pad area, posterior joint capsule parts and meniscus tissue parts were exempted by removing pixel value less than Otsu's threshold level (level 2). A morphological opening operation with structuring element of size 2 was also applied for filling the holes present in some areas of cartilage due to the thresholding operations.

(f) *Convex-hull and spline fitting operations to remove any leftover non cartilage tissues*: Sometimes, subchondral lesion area can merge with the superficial chondral tis-

sue, which cannot be removed completely by the previously mentioned steps. Therefore, for such cases two additional operations were applied. Firstly, a convex hull was fitted to the inner and outer cartilage boundary using 'convhull' routine in MATLAB 2016b (The MathWorks Inc., Natick, MA, USA 2016). This operation resulted in removal of any leftover non-cartilage tissues. In the second step, inner and outer cartilage boundary points were connected separately (Fig. 1q) and developed two masks with the help of cubic spline interpolation-based curve fitting process. Finally, cartilage was segmented from those masks by applying the exclusive-OR operation. The resultant mask (mask-2) was multiplied with the corresponding FS-PD-FSE image (Fig. 1r). Key steps of the segmentation process using radial search and the proposed method are shown in Fig. 1.

The proposed segmentation approach was also used for the cartilage segmentation on T2-weighted images with the following changes. Initially, the proposed pre-processing method was applied on T2-weighted images corresponding to TE = 6.4 ms (short), TE = 25.6 ms (intermediate) and TE = 51.2 ms (long) sequentially for evaluating the performance of pre-processing techniques with these images. Image with long TE was provided best performance and used for further segmentation process. The intensities above the Thresh-1 value were selected as zero. The mask (mask-1) generated from the radial-search method was applied on T2-weighted and T2 map generated from multi-echo T2 values by fitting monoexponential function given as follows:

$$S(TE) = S_0 \times e^{-(TE/T2)} + c \tag{3}$$

where S(TE) is the signal intensity of T2-weighted image at echo time TE [11] and T2, S_0 and c are parameters to be estimated. In T2 map, the two-level Otsu's thresholding steps were carried out by using two predefined T2 (in ms) threshold values. From the T2 map, synovial fluid, Hoffa's fat pad and chemical shift artefact area were removed by setting pixel value greater than 70 ms equal to zero. Also, the presence of meniscus tissue area and posterior joint capsule area was removed by setting pixel value less than 15 ms equal to zero.

The above procedures were also applied for tibial cartilage segmentation. Finally, we get separate masks for femur–tibia cartilage. There could be overlap among tibial and femoral cartilage in the weight-bearing area. A tangent line was used to separate the femoral and tibial cartilage component using the two end points of the overlapping zone; end points for overlapping zone were automatically detected using vertical line search operation.

Statistical validation

The accuracy of the proposed segmentation approach was evaluated using manual segmented ground truth cartilage. For validation, dice coefficient (DC) [12], Jaccard coefficient (JC) [13] and sensitivity index (SI) [14] were computed using the following expression:

$$\mathrm{DC} = (2(|A \cap B|))/(|A| + |B|) \tag{4}$$

$$\mathrm{JC} = (|A \cap B|)/(|A| + |B| - |A \cap B|) \tag{5}$$

$$\mathrm{SI} = (|A \cap B|)/|B| \tag{6}$$

where A is the manually segmented cartilage mask developed by the radiologist and B is the segmented cartilage using the proposed method. Two consecutive slices from the subchondral abnormality area of SBA patients/normal slices from without SBA patients were selected for the evaluation. Also, segmentation results of five patients data (3 SBA and 2 without SBA) were evaluated using 3D masks. For inter-reader variability testing, similarity measures were calculated based on reader 1 segmentation masks *vs* the proposed method-based mask and reader 2 segmentation mask *vs* the proposed method-based mask. Inter-reader variability was calculated based on those similarity measures using the coefficient of variation (CV) approach, which is defined as

$$\mathrm{CV} = \left(\frac{\text{Standard Deviation}}{\text{Average}}\right) \times 100 \tag{7}$$

For evaluating the statistical significance of difference between radial-search and modified radial-search method, Wilcoxon signed-rank test was applied. All statistical analyses were done with IBM SPSS Statistics® (version 15.0, Armonk, NY) software package and Microsoft Excel® (Microsoft Corp., Redmond, WA, USA) software.

2D visualization framework

The technique used for the projection of whole cartilage present in a patient data on a 2D plane is called 2D WearMap [4]. In this study, mainly two separate 2D WearMaps were generated from the segmentation results using T2 values and thickness values. 2D thickness WearMap was developed based on radial line method with single degree increment from 0° to 180°. Cartilage thickness was measured using the formula:

$$D = \sqrt[2]{\left(X_{\mathrm{op}} - X_{\mathrm{ip}}\right)^2 + \left(Y_{\mathrm{op}} - Y_{\mathrm{ip}}\right)^2} \tag{8}$$

where (X_{ip}, Y_{ip}) is the inner (bone–cartilage) boundary pixel coordinates and (X_{op}, Y_{op}) is the corresponding outer (cartilage–cartilage) boundary pixel coordinates. For getting better visualization, the map was smoothened by 3 × 3 kernel and interpolates the slices. Procedure for the thickness and T2 map 2D WearMap generation is illustrated in Fig. 2. Cartilage thickness was measured in mm by multiplying D value within plane resolution of the data.

Results

In this study, tibiofemoral cartilage of 20 OA subjects without SBA and 9 OA subjects with SBA was segmented successfully using the proposed modified radial-search method. DC-based inter-reader CV for femur cartilage was 4.18 ± 3.18% (with SBA) and 3.40 ± 2.12% (without SBA), and for tibia cartilage, it was 4.58 ± 3.26% (without SBA), respectively. All the statistical validation result of the current study was done by using reader 1 manual segmentation mask.

Figure 3 shows the segmentation results of representative patients having SBA lesions. Row I shows the patient data having chondral thinning with a subchondral cystic change in the antero-inferior area of femur bone above the Hoffa's fat pad in the lateral side. Row II shows data of a patient having subchondral abnormality near the antero-inferior area of femur bone in the lateral side. Row III shows data of a patient having small area of avascular necrosis present in the inferior area of femur bone in medial side. Images in column II represent the manually segmented cartilage masks as a reference. For these representative patients, radial-search approach failed to segment cartilage near SBA lesion as shown in column III. Modified radial-search approach successfully segmented the entire cartilage as shown in column IV.

Figure 4 shows the example of segmentation performance on multiple slices of one OA subject without SBA in the image data set. Representative images were selected from lateral, central and medial slices. In this subject, the DC value of segmented femur cartilage was 87.0 ± 1.4% and tibial cartilage was 84.0 ± 1.4%, respectively. Figure 5 shows the example of segmentation performance on one OA subject with SBA present in the antero-inferior area of femur cartilage in the lateral compartment, and the DC value of segmented femur cartilage was 82.5 ± 2.1% and tibial cartilage was 80.5 ± 4.9%, respectively.

The DC value of all subjects having femur bone abnormality (nine subjects) using radial-search method was 64.6 ± 7.8%, and using modified approach, it was 81.4 ± 2.8%, respectively. Wilcoxon signed-rank test shows that DC was significantly ($P \leq 0.05$) higher for the proposed modified cartilage approach compared to reported radial-search approach. The DC result of subjects of femur cartilage without SBA (twenty subjects) was 82.5 ± 4.5% and 84.8 ± 2.0% using radial-search method and modified method, respectively. The difference between these DC values was not statistically significant ($P = 0.0625$). Figure 6 shows the box and whisker plots of the statistical validation results (DC, JC, SI) of femur cartilage segmentation.

Similarly, DC values for tibial cartilage in all subjects were 80.4 ± 1.6% using radial-search method and 81.9 ± 2.4%

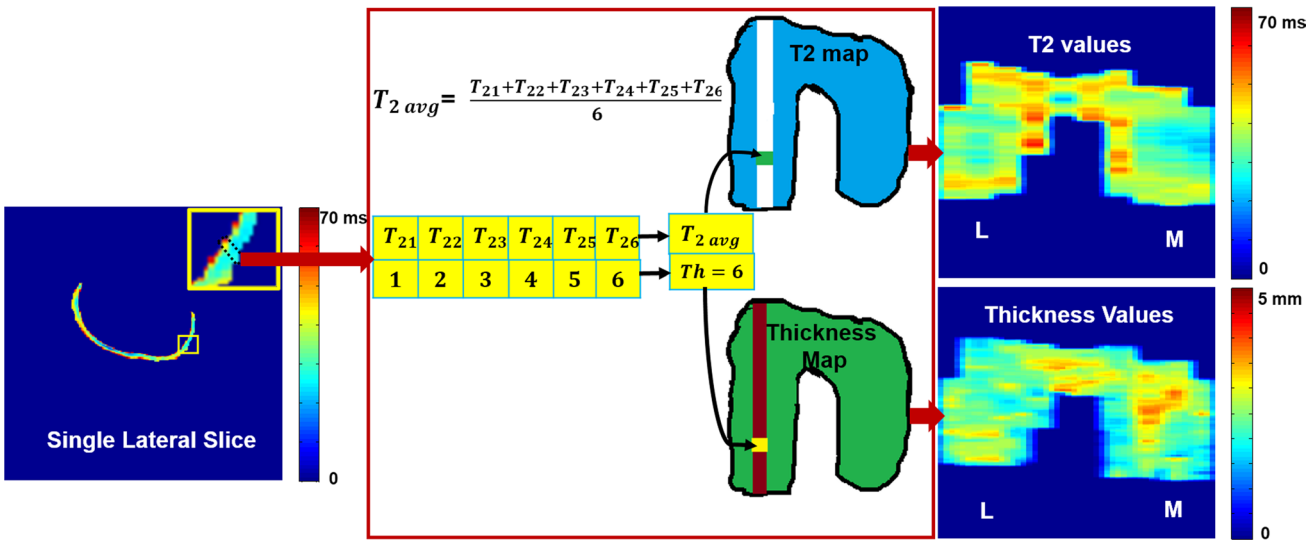

Fig. 2 Illustration of 2D WearMap generation from the segmented cartilage. $T_{21,}$ T_{22}…T_{26} are the individual pixel T2 values, and Th is the total number of pixels along the selected radial line. In 2D WearMap of T2 values and thickness values, *L* represents the lateral compartment region and M represents the medial compartment region of the cartilage

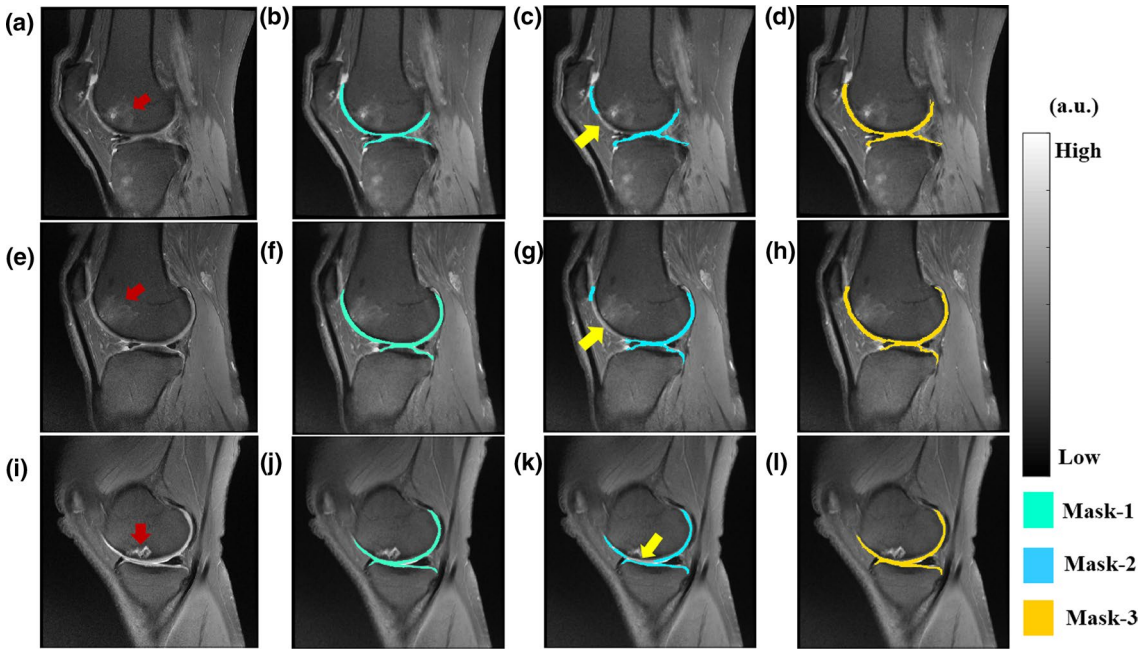

Fig. 3 Tibiofemoral cartilage segmentation results of 3 patients data (rows I, II and III) having subchondral bone abnormality. Column I shows the FS-PD-FSE-weighted images of patient data [red arrows in (**a**, **e**, **i**) indicate the presence of subchondral bone abnormality], column II shows the overlay of manual segmented cartilage masks (mask-1) (**b**, **f**, **j**), column III shows the overlay of segmentation mask (mask-2) using radial-search method [yellow arrows in (**c**, **g**, **k**) indicate the missed chondral area superficial to the subchondral abnormality], and column IV images (**d**, **h**, **l**) show the overlay of the segmented tibiofemoral cartilage mask (mask-3) using modified radial-search method. The scale shows the image intensity of FS-PD-FSE images and (a.u.) represents arbitrary unit

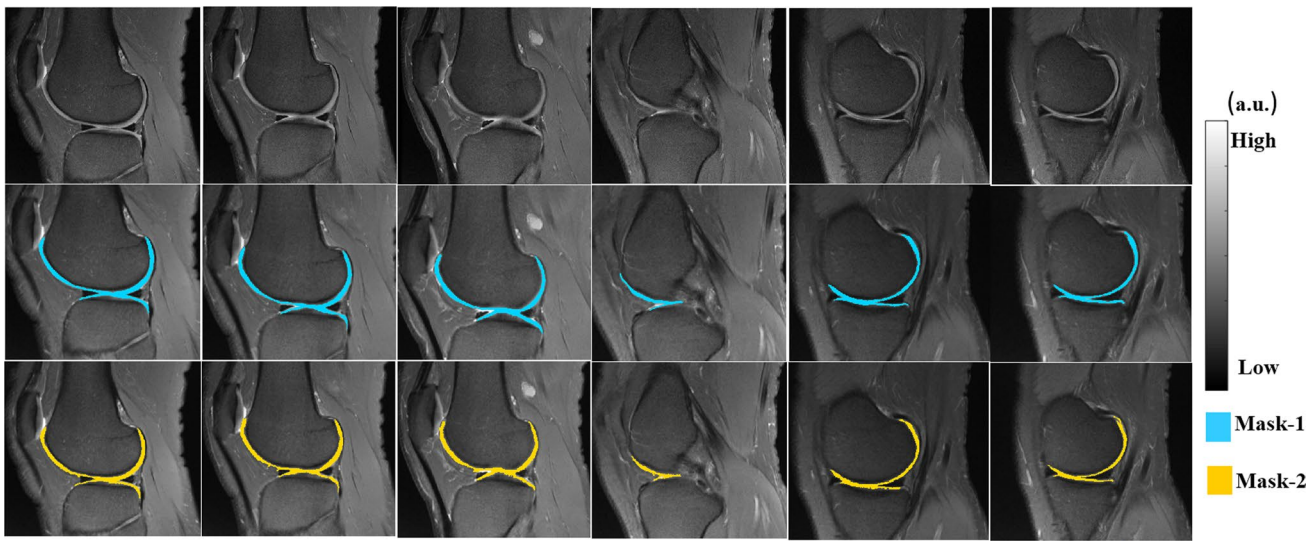

Fig. 4 Performance of modified radial-search-based algorithm for multiple slices of one OA patient without SBA in the FS-PD-FSE image data set. Row I images represent the selected slices of FS-PD-FSE image data, row II images represent the overlay of manual drawn segmentation mask (mask-1), and row III images represent the overlay of segmentation mask (mask-2) obtained from the proposed method. The scale shows the image intensity of FS-PD-FSE images and (a.u.) represents arbitrary unit

using modified radial-search method. For tibia cartilage, the DC values using the proposed modified radial search were slightly higher compared to radial-search approach and the difference was statistically significant ($P \leq 0.05$). JC values for tibial cartilage in all OA patients were $69.1 \pm 3.5\%$ using radial-search method and $69.5 \pm 3.8\%$ using modified method. Similarly, SI values for tibial cartilage in all patients were $75.4 \pm 5.1\%$ using radial-search method and

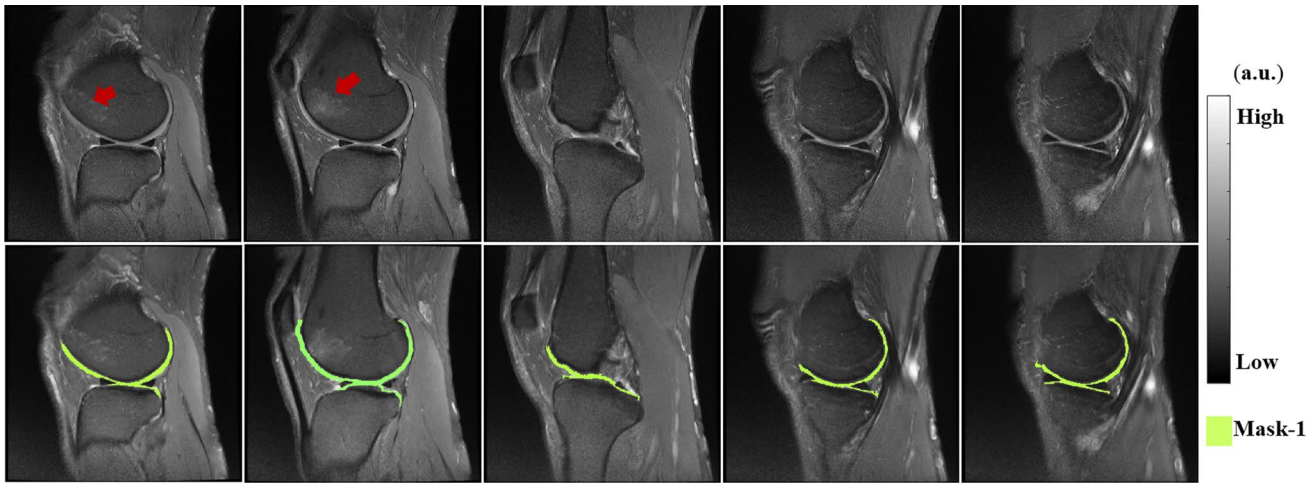

Fig. 5 Performance of modified radial-search-based algorithm for multiple slices of one OA patient with SBA (red arrow indicates the presence of SBA) in the FS-PD-FSE image data set. Row I images represent the selected slices of FS-PD-FSE image data, and row II images represent the overlay of segmentation mask (mask-1) obtained from the proposed method. The scale shows the image intensity of FS-PD-FSE images and (a.u.) represents arbitrary unit

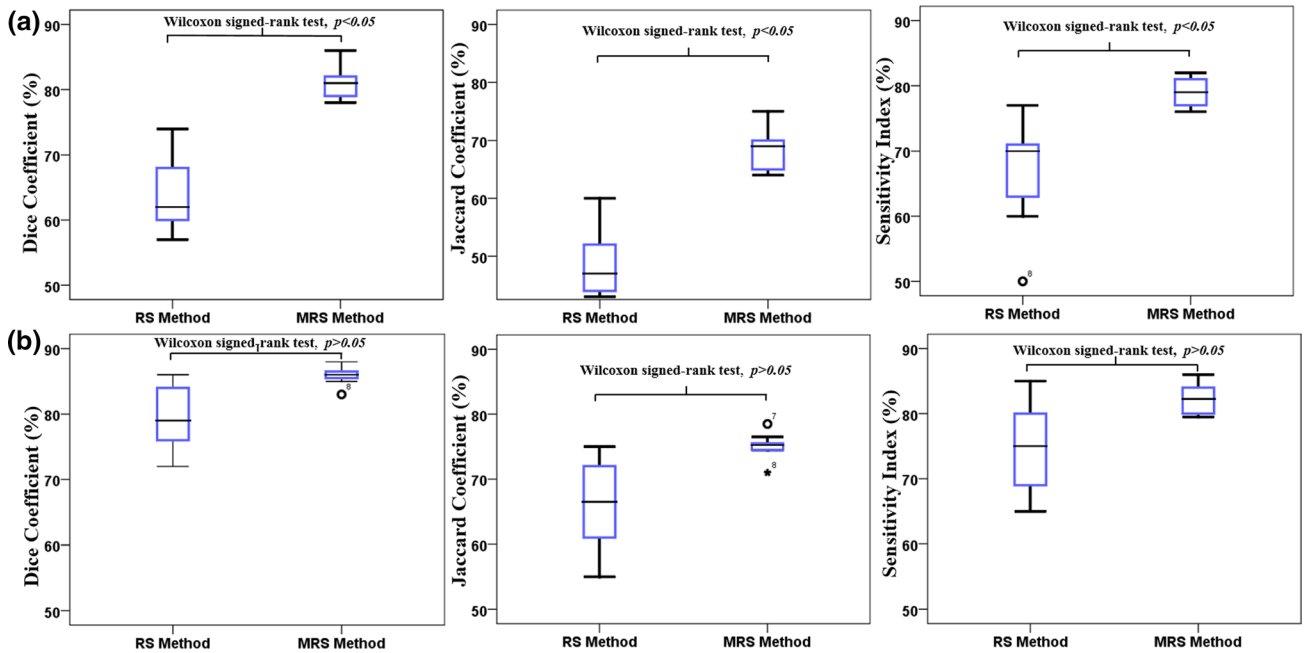

Fig. 6 Box and whisker plots of dice coefficient (DC), Jaccard coefficient (JC) and sensitivity index (SI) corresponding to segmented femur cartilage in OA patient data with subchondral bone abnormality (**a**) and without subchondral bone abnormality (**b**) using radial-search (RS) and the proposed modified radial-search (MRS) method

81.0 ± 4.9% using modified method. Comparison of different tibiofemoral cartilage segmentation studies relevant to the proposed study is presented in Table 2.

The DC values for the segmentation results of five OA patients with 3D masks were 81.8 ± 2.8% (femur cartilage) and 81.0 ± 2.2% (tibial cartilage), respectively. The JC values for the cartilage segmentation were 69.3 ± 3.9% (femur cartilage) and 68.6 ± 3.1% (tibia cartilage), respectively. Similarly, SI values for segmented femur cartilage were 78.7 ± 3.9%, and for tibial cartilage, it was 79.4 ± 2.9% using modified radial-search method.

Similar segmentation results were also obtained from the T2-weighted images. The DC value of all subjects having femur bone abnormality (nine subjects) using radial-search

Table 2 DC comparison of different automatic methods of cartilage segmentation

SI no.	Authors	Method	Modalities	Template image	Average DC (%)	
					Femur	Tibia
1	Folkesson et al. [21]	*k*-NN classification	Turbo 3D T1 sequence	Used	77	81
2	Fripp et al. [26]	Deformable model	T1-weighted FS-SPGR sequence	Used	85	82
3	Yin et al. [24]	Layered optimal graph	DESS sequence with water excitation	Used	84	80
4	Pang et al. [22]	Pattern recognition	FS T2-weighted images	Used	84	78
5	Chunsoo Ahn et al. [25]	Adaptive force function and template	3D DESS sequence with water excitation	Used	87	81.7
6	Liukkonen et al. [5]	Intensity profile-based radial search	3D PD TSE SPAIR, 3D PD FSE, 3D T2 GE	Unused	86	88
7	Proposed method	Modified radial search	FS-PD-FSE/T2-weighted	Unused	85	84

method was $63.3 \pm 11.1\%$, and using modified approach, it was $83.4 \pm 3.1\%$, respectively. The DC result of subjects of femur cartilage without SBA (twenty subjects) was $88.0 \pm 2.2\%$ using modified method. Similarly, DC values for tibial cartilage were $85.3 \pm 3.4\%$ using modified method.

Discussion

In this study, we have successfully developed and tested a semi-automated modified radial-search tibiofemoral cartilage segmentation approach that has been evaluated on MRI data set of 20 OA patients without SBA and 9 OA patients with SBA. Previously, reported study has shown that radial-search-based algorithm performed well for cartilage segmentation in healthy volunteers as well as OA patients [4]. This reported study tested two OA patient data without any SBA, and the sensitivity results of those patient data were less than 75% due to cartilage deformations. In the current study, the limitations of radial-search segmentation of tibiofemoral cartilage of OA patient with and without SBA were addressed.

Modified radial-search method successfully tested with OA patient data in general FS-PD-FSE sequence images which provide structural information of cartilage as well as on T2-weighted images without fat saturation corresponding to multiple echo times which provide structural and biochemical changes of cartilage [15, 16]. In routine clinical practice, for evaluating quantitative analysis of cartilage changes, clinicians manually insert multiple ROIs on different parts (weight bearing/non-weight bearing) of the cartilage T2 map of multiple slices. This task is tedious and prone to subjectivity, which can be overcome with the help of automatic segmentation procedure [17].

In the proposed modified radial-search method, for obtaining the femur and tibial seed point (SP1 and SP2), four pixels were manually selected from the central slice of lateral compartment. Since these pixel locations are clearly identifiable, subjectivity in seed point selection is quite low. This is the only stage of user input throughout the entire segmentation pipeline. Further development can be carried out to automatize the seed point selection. Recently, a preliminary study has proposed an automatic seed point selection procedure [18], which needs to be validated for FS-PD-FSE images and on large data sets. Since the BME lesion diameter > 20 mm is considered as grade III (severe) [19], the maximum area considered in the current study for connected component labelling was fixed accordingly. Therefore, the proposed modified radial-search method needs to be evaluated on severe SBA lesions with diameter > 20 mm.

The proposed approach worked well on FS-PD-FSE images and T2-weighted images which are acquired routinely for OA patients. We expect that the proposed method can be extended, with slight modifications, for images acquired using other sequences such as SPGR. In the current study, a part of SBA tissue was merged with the superficial chondral area in two patient data. In those cases, the modified radial-search method was successfully segmented the chondral tissue from the subchondral lesion area with convex-hull operation followed by curve fitting operation.

Several studies on cartilage segmentation have used template-based and machine learning algorithms; however, these methods required large training data set for the segmentation purpose [20–22]. Direct and reasonable comparison of different segmentation work is difficult since the MR sequence and study population are different. Most of the reported segmentation studies dealt with healthy volunteer subjects and limited studies discussed the segmentation of OA subjects especially data having advanced OA characteristics like SBA.

In the current study, statistical validation was done by using DC, JC and SI measurements. Both the femur and tibial DC results showed greater than or equal to 80% accuracy in both sequence images, which indicates a good

overlapping agreement of manual segmented mask with the proposed method mask. In femur cartilage segmentation, the DC accuracy of OA patient data with SBA was ~4% less compared to patient without SBA. One of the reasons of this accuracy reduction might be the patient data with SBA having advanced characteristics of OA. In our study, the performed inter-reader variability was < 5% which is comparable with reported studies [17].

In the current study, 2D WearMaps of cartilage thickness and T2 values were generated using segmented cartilage for better visualization. Reported study shows that easy identification of focal lesion/cartilage degradation was possible by using techniques such as colour map, scaling and thresholding of generated 2D map [4]. Also, cartilage anatomy-based subcompartmental classification (weight bearing, non-weight bearing, lateral, medial) and analysis could be possible by inserting different ROIs on 2D WearMap. Another study shows that the identification of approximate cartilage area affected by magic angle effect was easily located from the 2D WearMap-based evaluation [23].

We have tested the method on retrospective data, which had slice thickness of 4 mm. The same method can be applied for data with finer slice thickness, and results might further improve on finer slice thickness data. The time required for segmentation method depends upon number of slices. The time required for the manual selection of seed point was approximately 10 s per patient. The radial-search as well as modified radial-search method required 6–8 s for the segmentation of each slice on personal computed (Intel(R) Core(TM) i7-4770, 3.40 GHz CPU and 16 GB RAM). For the current study data, 15 slices, it took around 2.1 min. The time needed for the processing of T2 map generation was approximately 10 s per slice. Assuming manual cartilage segmentation requires around 1 min per slice, the proposed modified radial-search method is much faster compared to manual segmentation. Processing speed of the proposed modified radial-search method can further be improved by using better computer processor.

One of the limitations of this study is the manual selection of seed points. Another limitation is the absence of OA patient data having SBA in tibial bone.

In future, for getting a stable reliable validation, the proposed approach needs to be evaluated on a large number of patient data with different types of BME lesions in femur or tibial bone area and needs to be tested the performance of algorithm on femur–tibia cartilage using coronal view.

In conclusion, in the current study, a modified radial-search approach has been presented, particularly for OA patients with SBA. The proposed approach was successfully tested on conventional FS-PD-FSE images and multiple echo T2-weighted images for refinement of segmentation of cartilage.

Acknowledgements Authors acknowledge the MRI data acquisition support from Mahajan Imaging centre, New Delhi, India. The authors would like to thank Dr. Harsh Mahajan for providing the clinical insights, Ms. Madhuri Bansal, an application analyst in Mahajan Imaging Centre for her support in data collection.

Author contributions RT, AS and AM conceived and designed the experiments. RT, SPJ, SR and AS performed the experiments. RT, AS and SPJ analysed the data. RT, SPJ, SR, VKV, VM, AS and AM contributed materials/analysis tools. RT, SPJ, SR, VKV, VM, AS and AM contributed to the writing of the manuscript.

Funding This study was supported by the Industrial Research & Development Unit, Indian Institute of Technology Delhi (FIRP Project Number-MI01422). The funding body had no role in study design, data collection and analysis, decision to publish or preparation of the manuscript.

Compliance with ethical standards

Conflict of interest The authors declare that they have no conflict of interest.

Ethical approval This article does not contain any studies with animals performed by any of the authors.

Informed consent Informed consent was obtained from all individual participants included in the study.

References

1. Chen D, Shen J, Zhao W, Wang T, Han L, Hamilton JL, Im H (2017) Osteoarthritis: toward a comprehensive understanding of pathological mechanism. Bone Res 5:16044–16057
2. Gold GE, Chen CA, Koo S, Hargreaves BA, Bangerter NK (2009) Recent advances in MRI of articular cartilage. AJR Am J Roentgenol 193(3):628–638
3. Peuna A, Hekkala J, Haapea M, Podlipská J, Guermazi A, Saarakkala S, Nieminen MT, Lammentausta E (2018) Variable angle gray level co-occurrence matrix analysis of T 2 relaxation time maps reveals degenerative changes of cartilage in knee osteoarthritis: oulu knee osteoarthritis study. J Magn Reson Imaging 47(5):1316–1327
4. Akhtar S, Poh CL, Kitney RI (2007) An MRI derived articular cartilage visualization framework. Osteoarthr Cartil 15:1070–1085
5. Liukkonen MK, Mononen ME, Tanska P, Saarakkala S, Nieminen T, Korhonen RK (2017) Engineering application of a semi-automatic cartilage segmentation method for biomechanical modeling of the knee joint. Comput Methods Biomech Biomed Eng 5842:1–11
6. Poh C-L, Kitney RI (2006) Viewing interfaces for segmentation and measurement results. In: IEEE engineering in medicine and biology 27th annual conference, vol 5, pp 5132–5135
7. Hunter DJ, Zhang Y, Niu J, Goggins J, Amin S, LaValley MP, Guermazi A, Genant H, Gale D, Felson DT (2006) Increase in bone marrow lesions associated with cartilage loss: a longitudinal magnetic resonance imaging study of knee osteoarthritis. Arthritis Rheum 54:1529–1535
8. Kijowski R, Blankenbaker DG, Baer GS, Graf BK (2013) Evaluation of the articular cartilage of the knee joint: value of adding a T2 mapping sequence to a routine MR imaging protocol 1. Radiology 267:503–513

9. Liu F, Zhou Z, Jang H, Samsonov A, Zhao G, Kijowski R (2018) Deep convolutional neural network and 3D deformable approach for tissue segmentation in musculoskeletal magnetic resonance imaging. Magn Reson Med 79(4):2379–2391
10. Cohen ZA, McCarthy DM, Kwak SD, Legrand P, Fogarasi F, Ciaccio EJ, Ateshian GA (1999) Knee cartilage topography, thickness, and contact areas from MRI: in vitro calibration and in vivo measurements. Osteoarthr Cartil 7(1):95–109
11. Koff MF, Amrami KK, Kaufman KR (2007) Clinical evaluation of T2 values of patellar cartilage in patients with osteoarthritis. Osteoarthr Cartil 15:198–204
12. Dice LR (1945) Measures of the amount of ecologic association between species. Ecology 26:297–302
13. Jaccard P (1912) The distribution of the flora in the alpine zone. New Phytol XI:37–50
14. Udupa JK, Leblanc VR, Zhuge Y, Imielinska C, Schmidt H, Currie LM, Hirsch BE, Woodburn J (2006) A framework for evaluating image segmentation algorithms. Comput Med Imaging Graph 30:75–87
15. Mosher TJ, Dardzinski BJ (2004) Cartilage MRI T2 relaxation time mapping: overview and applications. Semin Musculoskelet Radiol 1:355–368
16. David-vaudey E, Ghosh S, Ries M, Majumdar S (2004) T2 relaxation time measurements in osteoarthritis. Magn Reson Imaging 22:673–682
17. Bae KT, Shim H, Tao C, Chang S, Wang JH, Boudreau R, Kwoh CK (2009) Intra-and inter-observer reproducibility of volume measurement of knee cartilage segmented from the OAI MR image set using a novel semi-automated segmentation method. Osteoarthr Cartil 17:1589–1597
18. Jogi SP, Rafeek T, Rajan S, Rangarajan K, Singh A, Mehndiratta A (2017) Automated seed points selection based radial-search segmentation method for sagittal and coronal view knee MRI imaging. In: 26th annual meeting ISMRM-ESMRMB. vol 2, pp 2017–2019
19. Kornaat PR, Sharma R, Botha-scheepers SA, Bloem JL (2007) Bone marrow edema-like lesions change in volume in the majority of patients with osteoarthritis; associations with clinical features. Eur Radiol 17:3073–3078
20. Stehling C, Baum T, Mueller-hoecker C, Liebl H, Carballido-Gamio J, Joseph GB, Majumdar S, Link TM (2011) A novel fast knee cartilage segmentation technique for T2 measurements at MR imaging data from the osteoarthritis initiative. Osteoarthr Cartil 19:984–989
21. Folkesson J, Dam EB, Olsen OF, Pettersen PC (2007) Segmenting articular cartilage automatically using a voxel classification approach. IEEE Trans Med Imaging 26:106–115
22. Pang J, Li P, Qiu M, Chen W, Qiao L (2015) Automatic articular cartilage segmentation based on pattern recognition from knee MRI images. J Digit Imaging 28:695–703
23. Kaneko Y, Nozaki T, Yu H, Chang A, Kaneshiro K, Schwarzkopf R, Hara T, Yoshioka H (2015) Normal T2 map profile of the entire femoral cartilage using an angle/layer dependent approach. J Magn Reson Imaging 42(6):1507–1516
24. Yin Y, Zhang X, Williams R, Wu X, Anderson DD, Sonka M (2010) LOGISMOS—layered optimal graph image segmentation of multiple objects and surfaces: cartilage segmentation in the knee joint. IEEE Trans Med Imaging 29(12):2023–2037
25. Ahn C, Bui TD, Lee Y, Shin J, Park H (2016) Fully automated, level set based segmentation for knee MRIs using an adaptive force function and template: data from the osteoarthritis initiative. Biomed Eng Online 15(1):99
26. Fripp J, Crozier S, Warfield SK, Member S, Ourselin S (2010) Automatic segmentation and quantitative analysis of the articular cartilages from magnetic resonance images of the knee. IEEE Trans Med Imaging 29:55–64